Laser and Particle Beams (2017), *35*, 337–343.

doi:10.1017/S0263034617000258

Influence of Au M-band flux asymmetry on implosion symmetry

S. JIANG,[1,2] L. LI,[1] L. JING,[1] L. KUANG,[1] H. LI,[1] L. ZHANG,[1] Z. LIN,[1] AND Y. DING[1,2]

[1]Research Center of Laser Fusion, China Academy of Engineering Physics, Mianyang, 621900, People's Republic of China
[2]Center for Applied Physics and Technology, Peking University, Beijing, 100871, People's Republic of China

(Received 18 December 2016; Accepted 14 March 2017)

Abstract

In indirect-drive inertial confinement fusion, the radiation symmetry must be controlled for the achievement of hotspot ignition. The radiation symmetry is of great importance. In this paper, we investigate the drive asymmetry of the M-band (2–5 keV) radiation emitted from an Au holhraum wall by using the three-dimensional view-factor code IRAD3D. Analysis of the M-band flux drive at the Shenguang-III laser facility shows that it is asymmetric and that the asymmetry varies with time. For a given cross section over the pole, the initial M-band flux asymmetries are $P_2 = 11.59$, $P_4 = 1.41$, and $P_6 = -0.64\%$. When the asymmetries are artificially added to a symmetric radiation drive, the position of the deuterium-tritium (DT) ice/gas interface is asymmetric for a National Ignition Facility capsule in 1D simulation. This means that M-band flux asymmetry can lead to implosion asymmetry even if the total radiation is symmetric. Pure CH and Si-doped CH capsules are considered. The results show that a mid-Z dopant can partly reduce the asymmetry. However, the asymmetry is still very large. Thus, it is necessary to study the M-band flux asymmetry and its influence on the implosion symmetry.

Keywords: Holhraum; Au M-band; Flux asymmetry; Pure CH and Si-doped CH capsules; Implosion symmetry

1. INTRODUCTION

Implosion symmetry is a key issue for indirect-drive inertial confinement fusion (ICF) (Lindl, 1995; Lindl, & Moses, 2011). It is seriously affected by radiation symmetry. For this reason, control of the radiation symmetry is crucial (Ramirez *et al*., 1998). In a hohlraum, laser energy is absorbed by the high-Z wall, such as Au, and converted into X-ray radiation drive. The radiation drive is always asymmetric (Schnittman & Craxton, 1996) and varies with time (Kyrala *et al*., 2011). The tolerable radiation asymmetry in an implosion is no more than 1–2% (Murakami & Meyer-Ter-Vehn, 1991; Murakami, 1992). Numerous experiments have been performed to study the measurement and control of the radiation symmetry. Capsule X-ray emission has been used to measure the radiation drive asymmetry (Dewald *et al*., 2013; Lindl *et al*., 2014). In addition, the radiation symmetry has been studied via charged-particle spectroscopy (Merrill, 2015). The radiation symmetry can be controlled by adjusting the position of the laser-beam spots (Delamater *et al*., 2000), by tuning the relative power (Meezan *et al*., 2010) or laser wavelength between the inner and the outer beams.

Radiation symmetry is a complex and difficult topic (Ramirez *et al*., 1998). Detailed information about radiation symmetry cannot be easily obtained experimentally. Thus, studies on radiation symmetry often involve numerical simulation (Ramis *et al*., 2014). Numerical simulations have shown that radiation asymmetries occur at the first 2 ns and that the peak of the laser drive can seriously affect the implosion symmetry (Dewald *et al*., 2011). Experiments have been designed for measuring and tuning the early-time symmetry (Magelssen *et al*., 1998; Landen *et al*., 2011; Dewald *et al*., 2013). Owing to the development of two-dimensional (2D) (Ramis *et al*., 2009) and three-dimensional (3D) (Ramis *et al*., 2014) numerical-simulation code, simulation of radiation symmetry is possible. The view-factor code VISRAD (MacFarlane *et al*., 2005) and IRAD3D (Jiang *et al*., 2014; Jing *et al*., 2015) are used to analyze the radiation conditions. The 3D HYDRA (Marinak *et al*., 2001) and MULTI (Ramis, 2013) codes are important for simulating the hydrodynamics process. It is the foundation for the numerical simulation of

Address correspondence and reprint requests to: S. Jiang, Research Center of Laser Fusion, China Academy of Engineering Physics, P. O. Box 919-986, Mianyang, 621900, People's Republic of China. E-mail: jiangshn@vip.sina.com

radiation symmetry. Qualitative analysis by simulation is useful for the study of implosion symmetry.

Numerous studies have focused on the measurement and control of the total radiation flux symmetry (Delamater *et al.*, 1996). The study of the M-band flux asymmetry is also important. M-band X rays play an important role in ICF and can lead to a preheating effect. The preheating effect cannot be avoided, because of these high-energy X rays. It can only be reduced by using a mid-Z dopant (Robey *et al.*, 2005; Simakov *et al.*, 2014). Different methods have been employed for measuring the M-band fraction (Li *et al.*, 2010, 2014), reducing the M-band fraction (Li *et al.*, 2010), and restraining the transmission of M-band X rays (Li *et al.*, 2014). Varnum mentioned that M-band flux asymmetry resulted in the asymmetric preheating of a capsule. This may have affected the achievement of ignition (Varnum *et al.*, 2000). In this study, the M-band flux asymmetry was examined in detail. By using the 3D view-factor code IRAD3D, we determined the M-band flux asymmetry for a typical Shenguang-III hohlraum (Jing *et al.*, 2015). When the asymmetry was artificially added to a symmetric radiation drive, the implosion analyzed via one-dimensional (1D) simulation became asymmetric. This means that the M-band flux asymmetry can lead to implosion asymmetry even though the total radiation is symmetric. The use of a Si dopant cannot prevent the asymmetry. Because of this characteristic, it is necessary to study the M-band flux asymmetry and its influence on the implosion symmetry.

2. M-BAND FLUX ASYMMETRY

In this section, the M-band flux asymmetry of the Shenguang-III hohlraum is discussed. The hohlraum design is similar to that used in the National Ignition Campaign (NIC) (Haan *et al.*, 2011); it is 2 mm in diameter, is 3.7 mm long, and has a laser entrance hole (LEH) 1.2 mm in diameter. The capsule is 0.8 mm in diameter. The hohlraum-to-capsule radius ratio is 2.5, according to the capsule design of the NIC. The Shenguang-III laser facility has 48 laser beams designed in four cones (28.5°, 35°, 49.5°, 55°) (Jing *et al.*, 2015). A schematic of the 48 laser beams is shown in Figure 1. In our discussion, each laser beam has an energy of 1000 J and provides a 1-ns input pulse with a wavelength of 0.351 μm. A continuous-phase plate is used for beam smoothing. The laser spots focusing on the LEH plane are round and 500 μm in diameter. The positions of the laser spots are shown in Figure 1. The calculation of the M-band flux asymmetry is based on the laser-spot position. The navy blue and watchet blue laser spots correspond to inner beams, with incident angles of 28.5° and 35°, respectively. The yellow and red laser spots correspond to outer beams, with incident angles of 49.5° and 55°, respectively.

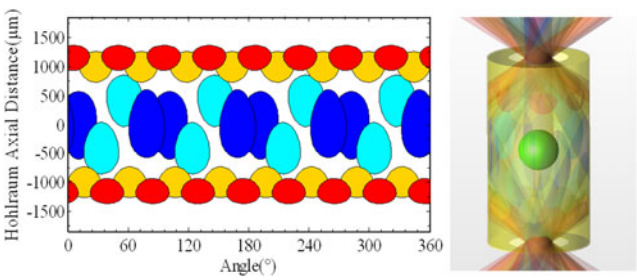

Fig. 1. Laser spots on the hohlraum wall for the Shenguang-III cylindrical hohlraum (left) and a schematic of the laser beams (right).

M-band X-rays are generated in and near the coronal plasma (Olson *et al.*, 2003). This results in an asymmetric M-band flux drive. When discussing the M-band flux asymmetry, we only consider the contribution of the laser spots. The laser beams are all assumed to be converted into M-band X rays when the normalized M-band flux drive distribution on the capsule is discussed. The distribution is shown in Figure 2. It is the result in the initial time. The 3D graph presents the visual M-band flux asymmetry. It is almost symmetric in the equatorial direction. The main asymmetry occurs in the polar direction. The minimum M-band flux occurs at points with $\theta = 0°$ or 180° and faces the LEH. A 2D contour map is shown in Figure 2b. This provides a numerical description of the normalized M-band flux. Obviously, the M-band flux drive is asymmetric.

The positions of the laser spots on a hohlraum are not fixed. The laser spots move with time. Usually, the motion of the laser spots results from wall motion (Huser *et al.*, 2009). The speed of the inward wall motion is assumed to be 200 μm/ns. The variable M-band flux drive distribution due to the spot motion is shown in Figure 3. At 0.3 ns, the distribution was similar to that at the beginning. However, the M-band flux became asymmetric in the equatorial direction, especially in the cross section near the equator. Until 1 ns, the positions of the peak and minimum M-band fluxes were exchanged, and the M-band flux asymmetry was large. Obviously, the M-band flux asymmetry varied with time. This asymmetry may grow larger as the laser spots move with time. This complicates the quantitative analysis of the M-band flux asymmetry.

We examined the influence of the M-band flux asymmetry on the implosion symmetry via 2D analysis. As previously mentioned, the M-band flux asymmetry varies with time. To simplify the discussion, we ignore the time variation and consider only the M-band flux asymmetry at the beginning. Figure 4 shows the normalized M-band flux drive distribution for a given cross section extracted from Figure 2. Figure 4b shows a cross-sectional schematic of the capsule. This is the cross section over the pole with $\varphi = 2.5°$ and 182.5°. The normalized angular distribution of the M-band flux drive for the cross section is shown in Figure 4a. It is taken from a point every 5° from 2.5°. The distance to the origin is the normalized M-band flux intensity. The M-band flux asymmetries are $P_2 = 11.59\%$, $P_4 = 1.41\%$, and $P_6 = -0.64\%$. The P_2 asymmetry is so large that it cannot be excluded.

https://doi.org/10.1017/S0263034617000258 Published online by Cambridge University Press

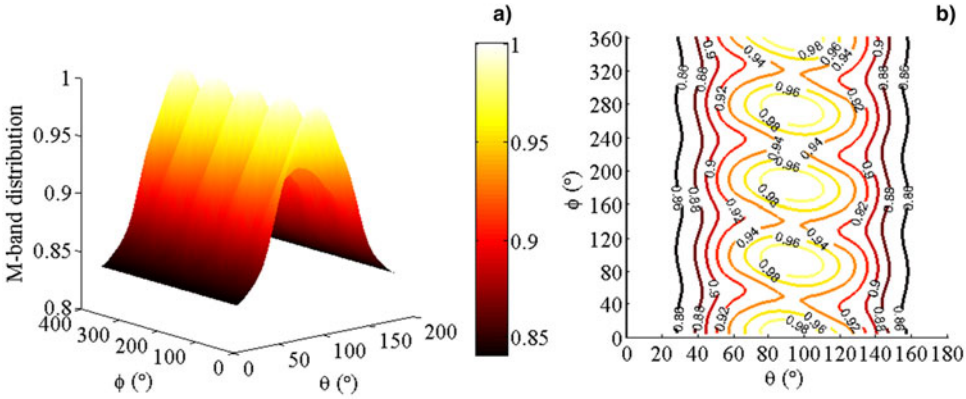

Fig. 2. Normalized M-band flux drive distribution on a capsule (0.8 mm in diameter): (a) 3D graph and (b) 2D contour map.

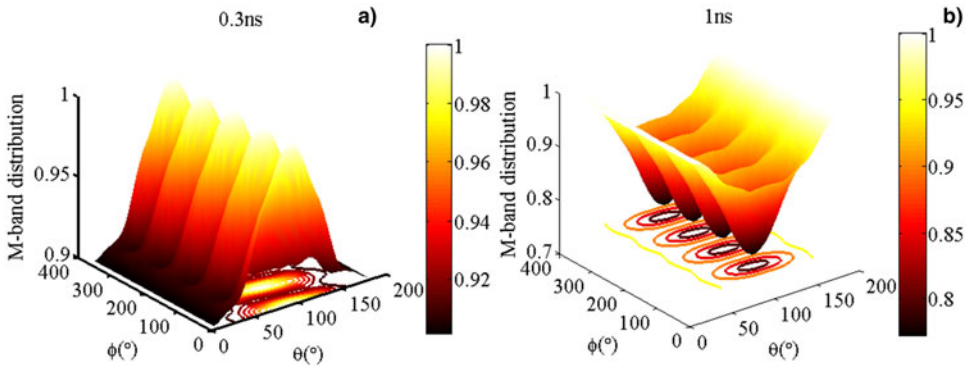

Fig. 3. Normalized M-band flux drive distribution at different times: (a) 0.3 ns and (b) 1 ns.

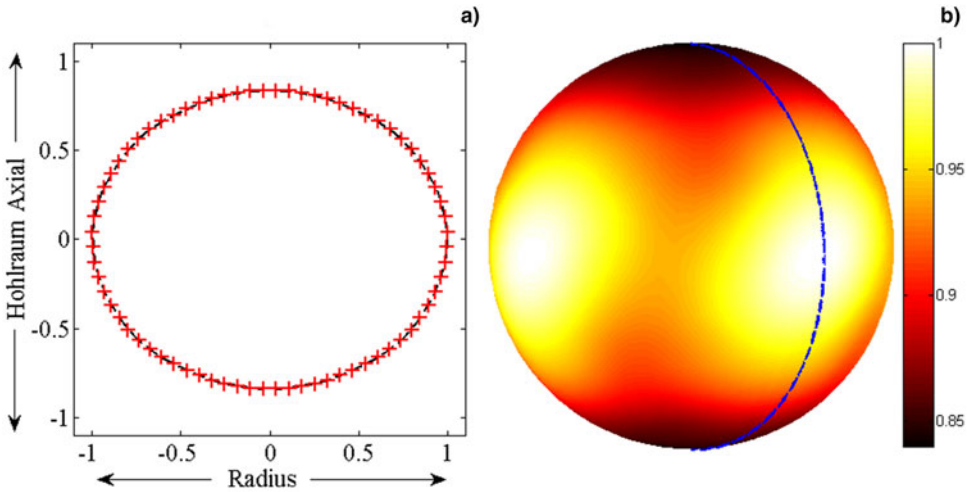

Fig. 4. Initial M-band flux drive distribution. (a) Normalized angular distribution of the M-band flux drive for a given cross section. The red crosses represent the intensity of the M-band flux drive at every point. (b) Schematic representation of the cross section (blue dashed line).

https://doi.org/10.1017/S0263034617000258 Published online by Cambridge University Press

M-band X rays are the key factor causing the preheating effect (Olson *et al.*, 2003). Although a mid-Z dopant can be used to reduce this effect, preheating is an important issue in ICF. Moreover, asymmetric M-band flux results in asymmetric preheating, which may lead to asymmetric implosion. Therefore, the study of the M-band flux asymmetry is necessary. We investigated the influence of the M-band flux asymmetry on the implosion symmetry by artificially adding the aforementioned M-band flux asymmetries to a symmetric radiation drive.

3. ONE-DIMENSIONAL SIMULATION

We investigated the influence of the M-band flux asymmetry on the implosion symmetry via simulation. As previously discussed, the M-band flux asymmetry varies with time, and the motion of the laser spots may affect the asymmetry. It is difficult to discuss the influence of the M-band flux asymmetry on the implosion symmetry if the time variation and the motion of the spots are considered. To simplify the analysis, we ignored these two factors. Because the lack of 2D simulation code, we used the 1D radiation hydrodynamic code MULTI (Ramis *et al.*, 1988; Eidmann *et al.*, 2000) to analyze the influence. For every point in Figure 4a, the implosion process was simulated by MULTI-1D. Here, we used the high-foot radiation drive (Dittrich *et al.*, 2014). The peak radiation temperature was 300 eV. The capsule size used in the simulation was the same as that of the high-foot capsule mentioned (Dittrich *et al.*, 2014), which had a 1130-μm outer radius. However, the ablator differed: it was pure CH.

For every point in Figure 4a, the radiation temperature is the same as the high-foot radiation drive. It reaches its peak about 13.5 ns. The distribution of the M-band fraction $f_m(i)$ is based on the normalized M-band flux intensity, with the highest M-band fraction being 15.0% (at equator) and the lowest M-band fraction being 12.6% (at pole). The radiations of two adjacent points exhibit little difference. The motion of the two points is continuous. Thus, the lateral mass flow in the capsule is ignored in our discussion. Because of the lack of National Ignition Facility hohlraum parameters, the distribution of the M-band fraction $f_m(i)$ at the peak radiation temperature is taken as that in Figure 4a. According to our previous study, the structure of the X-ray source is divided into two parts: the Planckian distribution and the Gaussian distribution (Li *et al.*, 2015). Fraction α mentioned in Li *et al.* (2015) differs from the M-band fraction f_m. As $T_R = 300$ eV, the relationship between $\alpha(i)$ and $f_m(i)$ can be written as $\alpha(i) = (f_m(i)–9.312)/79.15$ for every point. To simplify the simulation, $\alpha(i)$ was kept constant for the whole ignition time.

The 1D simulation result for every point was obtained using MULTI-1D. The density distribution at stagnation (14.5 ns) is shown in Figure 5. The large-amplitude P_2 asymmetry of the M-band flux induces a P_2 shape at stagnation. The P_2 distortion is apparent. A higher M-band fraction yields a higher ablation rate. The difference of the ablation rate at different points finally results in the P_2 distortion. Therefore, we should not overlook the influence of the M-band asymmetry when discussing the radiation symmetry.

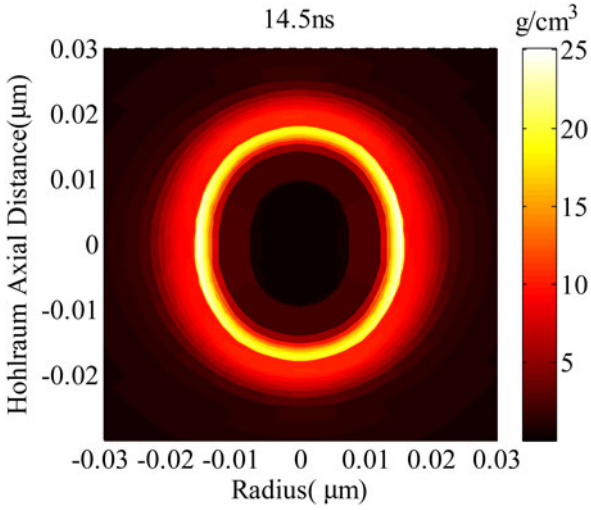

Fig. 5. Density distribution obtained from the 1D simulation.

In this study, the total radiation is symmetric. The only source of asymmetry is the M-band flux. Because of the large M-band flux asymmetry, the preheating of the ablator is asymmetric. This asymmetry leads to the final asymmetric compression. Briefly, the M-band flux asymmetry can lead to asymmetric implosion even though the total radiation is symmetric. This phenomenon should be noted. In the next section, it will be discussed by studying the shape of the deuterium-tritium (DT) ice/gas interface.

4. DISCUSSIONS

Obviously, the low-order mode shape of the pure CH capsule results from the large-amplitude P_2 asymmetry of M-band

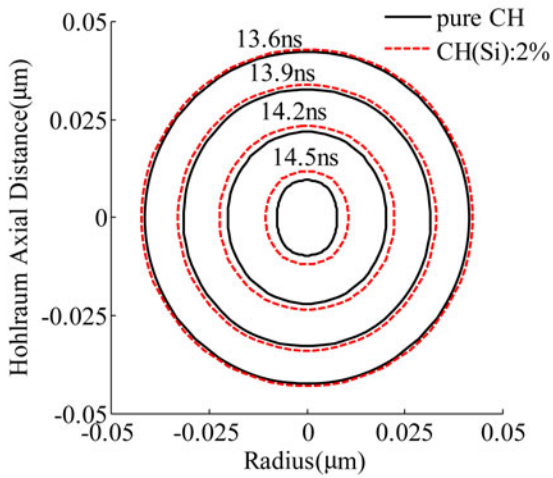

Fig. 6. Position of the DT ice/gas interface for the pure CH and Si-doped CH capsules at different times.

https://doi.org/10.1017/S0263034617000258 Published online by Cambridge University Press

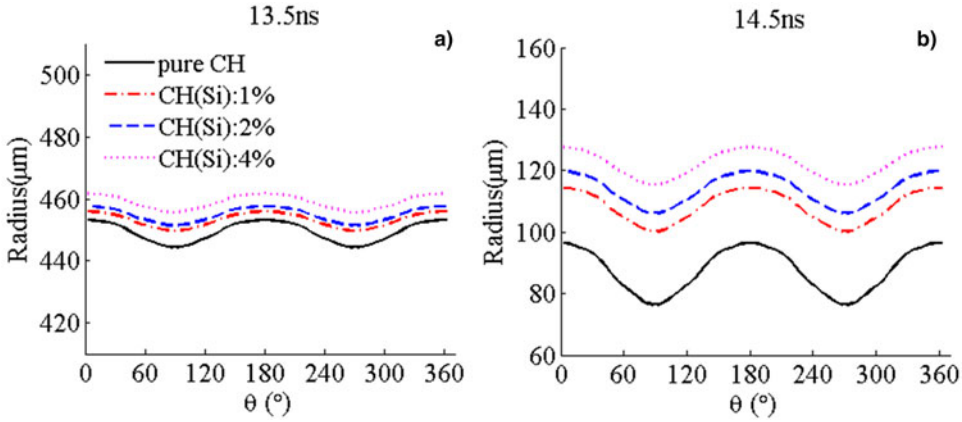

Fig. 7. Position of the DT ice/gas interface with respect to the polar angle: (a) at the peak radiation temperature and (b) at stagnation.

flux. A mid-Z dopant is necessary in the ignition target. A Si-doped CH capsule is considered in this section. It is a graded Si-doped capsule, which is the same as that of Dittrich *et al.* (2014). The doping fraction was stair-stepped as 1, 2, and 1% for the Si-doped CH capsule. Here, we discuss the shape of the DT ice/gas interface. This was obtained from the 1D simulation. The radiation source and structure are the same as those in the previous section.

Figure 6 shows the position of the DT ice/gas interface for the pure CH and Si-doped CH capsules at different times. The shape of the interface is clear from 13.6 ns (near the peak radiation temperature) to 14.5 ns (at stagnation). It changes with time. Initially, the low even-mode asymmetries are not large. However, they become larger with time, and the P_2 asymmetry becomes very large. The Si dopant can reduce this asymmetry. However, the P_2 asymmetry is still obvious.

Then, we changed the highest Si doping fraction (third layer of the ablator) from 1 to 4%. The symmetry was not improved. Figure 7 shows the position of the DT ice/gas interface with respect to the polar angle for different kinds of targets. The positions at the peak radiation temperature (13.5 ns) and at stagnation (14.5 ns) are discussed. The shape of the interface varies with time.

At the peak radiation temperature, the asymmetries are very similar between the pure CH and Si-doped capsules with different doping fractions. The P_4 and P_6 asymmetries are nearly zero, and the P_2 asymmetry is approximately 2%. This is reasonable. The asymmetric implosion is an accumulated process. The M-band flux intensity is low at a low radiation temperature, although α is fixed for the whole ignition time. Long-time asymmetric M-band flux leads to a large asymmetry. At stagnation, the asymmetries become obvious, as shown in Figure 7b. The Legendre low-order even modes P_0, P_2, P_4, and P_6 are listed in Table 1. The P_4 and P_6 asymmetries are not large (<2%); however, the P_2 asymmetry is very large. For the pure CH capsule, $P_2/P_0 = -14.22\%$. The P_2 asymmetry is reduced with the increase of the Si doping fraction. It is reduced from −8.19 to −6.25% as the highest Si doping fraction changes from 1 to 4%. P_0 increases because the capsule payload increases with the amount of the Si dopant. On the other hand, the Si dopant can smooth the asymmetric M-band flux, decreasing P_2. Therefore, P_2/P_0 is reduced by adding the Si dopant. However, this does not have a substantial impact. That is, the influence of the M-band flux asymmetry on the implosion symmetry is not negated by using a mid-Z dopant. This may be a serious problem in ICF. Consequently, it is of great importance to study the M-band flux asymmetry for the achievement of the final ignition.

Table 1. *Legendre low order even modes* P_0, P_2, P_4 *and* P_6 *at 14.5 ns*

Target type	P_0 (μm)	P_2 (μm)	P_2/P_0 (%)	P_4/P_0 (%)	P_6/P_0 (%)
Pure CH	90.6	−12.9	−14.22	−1.74	0.84
CH(Si):1%	110.3	−9.0	−8.19	−1.09	0.44
CH(Si):2%	115.8	−8.7	−7.53	−0.98	0.43
CH(Si):4%	124.0	−7.8	−6.25	−0.82	0.35

5. CONCLUSIONS

The M-band flux drive asymmetry for the Shenguang-III hohlraum and its influence on the implosion symmetry were qualitatively studied. The M-band flux drive is asymmetric. It varies with time owing to the laser-spot motion and can increase. For a given cross section over the pole, the initial M-band flux asymmetries are $P_2/P_0 = 11.59\%$, $P_4/P_0 = 1.41\%$, and $P_6/P_0 = -0.64\%$. The asymmetries are artificially added to a symmetric radiation drive. For every point, the implosion process is examined via 1D simulation. The results show that the implosion becomes asymmetric. The large M-band P_2 asymmetry leads to a large P_2 (−14.22%) asymmetry for a pure CH capsule at stagnation. A Si dopant can reduce the P_2 (~8%) asymmetry, but the asymmetry is still far from the requirement for ignition. This means that the M-band flux asymmetry can seriously

https://doi.org/10.1017/S0263034617000258 Published online by Cambridge University Press

affect the implosion symmetry even though the total radiation drive is symmetric. This may be the reason for the appearance of the implosion asymmetry.

On the other hand, the total radiation asymmetry and M-band flux asymmetry are time-dependent. The influence may be amplified in an ignition experiment. Therefore, the study of the M-band flux asymmetry is important. We must experimentally measure the M-band flux asymmetry. Future studies will consider the M-band flux asymmetry and focus on reducing its influence on the implosion symmetry. These studies may play a significant role in optimizing the implosion symmetry.

ACKNOWLEDGMENTS

The authors would like to thank the target fabrication and the laser operation staffs for their cooperation. This work was supported by the National Natural Science Foundation of China (Grant numbers 11475154 and 11405160) and the Foundation of China Academy of Engineering Physics (Grant no. 2013A0102002).

REFERENCES

Delamater, N.D., Lindman, E.L., Magelssen, G.R., Failor, B.H., Murphy, T.J., Hauer, A.A., Gobby, P., Moore, J.B., Gomez, V., Gifford, K., Kauffman, R.L., Landen, O.L., Hammel, B.A., Glendinning, G., Powers, L.V., Suter, L.J., Dixit, S., Peterson, R.R. & Richard, A.L. (2000). Observation of reduced beam deflection using smoothed beams in gas-filled hohlraum symmetry experiments at Nova. *Phys. Plasmas* **7**, 1609–1612.

Delamater, N.D., Magelssen, G.R. & Hauer, A.A. (1996). Re-emission technique for symmetry measurements in Hohlraum targets containing a centered high-Z ball. *Phys. Rev. E* **53**, 5240.

Dittrich, T.R., Hurricane, O.A., Callahan, D.A., Dewald, E.L., Döppner, T., Hinkel, D.E., Hopkins, L.F.B., Pape, S.L., MA, T., Milovich, J.L., Moreno, J.C., Patel, P.K., Park, H.S., Remington, B.A., Salmonson, J.D. & Kline, J.L. (2014). Design of a high-foot high-adiabat ICF capsule for the national ignition facility. *Phys. Rev. Lett.* **112**, 055002.

Dewald, E.L., Milovich, J.L., Michel, P., Landen, O.L., Kline, J.L., Glenn, S., Jones, O., Kalantar, D.H., Pak, A., Robey, H.F., Kyrala, G.A., Divol, L., Benedetti, L.R., Holder, J., Widmann, K., Moore, A., Schneider, M.B., Döppner, T., Tommasini, R., Bradley, K.D., Bell, P., Ehrlich, B., Thomas, C.A., Shaw, M., Widmayer, C., Callahan, D.A., Meezan, N.B., Town, R.P.J., Hamza, A., Dzenitis, B., Nikroo, A., Moreno, K., Wonterghem, B.V., Mackinnon, A.J., Glenzer, S.H., Macgowan, B.J., Kilkenny, J.D., Edwards, M.J., Atherton, L.J. & Moses, E.I. (2013). Early-time symmetry tuning in the presence of cross-beam energy transfer in ICF experiments on the National Ignition Facility. *Phys. Rev. Lett.* **111**, 235001.

Dewald, E.L., Milovich, J., Thomas, C., Kline, J., Sorce, C., Glenn, S. & Landen, O.L. (2011). Experimental demonstration of early time, hohlraum radiation symmetry tuning for indirect drive ignition experiments. *Phys. Plasmas* **18**, 092703.

Eidmann, K., Meyer-Ter-Vehn, J., Schlegel, T. & Hüller, S. (2000). Hydrodynamic simulation of subpicosecond laser interaction with solid-density matter. *Phys. Rev. E* **62**, 1202.

Haan, S.W., Lindl, J.D., Callahan, D.A., Clark, D.S., Salmonson, J.D., Hammel, B.A., Atherton, L.J., Cook, R.C., Edwards, M.J., Glenzer, S., Hamza, A.V., Hatchett, S.P., Herrmann, M.C., Hinkel, D.E., Ho, D.D., Huang, H., Jones, O.S., Kline, J., Kyrala, G., Landen, O.L., Macgowan, B.J., Marinak, M.M., Meyerhofer, D.D., Milovich, J.L., Moreno, K.A., Moses, E.I., Munro, D.H., Nikroo, A., Olson, R.E., Peterson, K., Pollaine, S.M., Ralph, J.E., Robey, H.F., Spears, B.K., Springer, P.T., Suter, L.J., Thomas, C.A., Town, R.P., Vesey, R., Weber, S.V., Wilkens, H.L. & Wilson, D.C. (2011). Point design targets, specifications, and requirements for the 2010 ignition campaign on the National Ignition Facility. *Phys. Plasmas* **18**, 051001.

Huser, G., Courtois, C. & Monteil, M.C. (2009). Wall and laser spot motion in cylindrical hohlraums. *Phys. Plasmas* **16**, 032703.

Jiang, S.E., Jing, L.F., Huang, Y.B. & Ding, Y.K. (2014). Novel free-form hohlraum shape design and optimization for laser-driven inertial confinement fusion. *Phys. Plasmas* **21**, 102710.

Jing, L.F., Jiang, S.E., Yang, D., Li, H., Zhang, L., Lin, Z.W., Li, L.L., Kuang, L.Y., Huang, Y.B. & Ding, Y.K. (2015). Angular radiation temperature simulation for time-dependent capsule drive prediction in inertial confinement fusion. *Phys. Plasmas* **22**, 022709.

Kyrala, G.A., Kline, J.L., Dixit, S., Glenzer, S., Kalantar, D., Bradley, D., Izumi, N., Meezan, N., Landen, O., Callahan, D., Weber, S.V., Holder, J.P., Glenn, S., Edwards, M.J., Koch, J., Suter, L.J., Haan, S.W., Town, R.P.J., Michel, P., Jones, O., Langer, S., Moody, J.D., Dewald, E.L., Ma, T., Ralph, J., Hamza, A., Dzenitis, E. & Kilkenny, J. (2011). Symmetry tuning for ignition capsules via the symcap technique. *Phys. Plasmas* **18**, 056307.

Landen, O.L., Edwards, J., Haan, S.W., Robey, H.F., Milovich, J., Spears, B.K., Weber, S.V., Clark, D.S., Lindl, J.D. & Macgowan, B.J. (2011). Capsule implosion optimization during the indirect-drive National Ignition Campaign. *Phys. Plasmas* **18**, 051002.

Li, L.L., Jiang, S.E., Zhang, L., Zheng, J.H., Qing, B., Zhang, J.Y., Kuang, L.Y. & Li, H. (2015). The importance of the transmission flux in evaluating the preheat effect in x-ray driven ablation. *Phys. Plasmas* **22**, 022702.

Li, L.L., Zhang, L., Jiang, S.E., Guo, L., Qing, B., Li, Z.C., Zhang, J.Y., Yang, J.M. & Ding, Y.K. (2014). The M-band transmission flux of the plastic foil with a coated layer of silicon or germanium. *Appl. Phys. Lett.* **104**, 054106.

Li, X., Lan, L., Meng, X., He, X., Lai, D. & Feng, T. (2010). Study on Au+ U+ Au sandwich Hohlraum wall for ignition targets. *Laser Part. Beams* **28**, 75–81.

Lindl, J.D. (1995). Development of the indirect-drive approach to inertial confinement fusion and the target physics basis for ignition and gain. *Phys. Plasmas* **2**, 3933–4024.

Lindl, J.D., Landen, O., Edwards, J., Moses, E. & NIC TEAM (2014). Review of the national ignition campaign 2009–2012. *Phys. Plasmas* **21**, 020501.

Lindl, J.D. & Moses, E.I. (2011). Special topic: Plans for the National Ignition Campaign (NIC) on the National Ignition Facility (NIF): On the threshold of initiating ignition experiments. *Phys. Plasmas* **18**, 050901–050902.

Macfarlane, J.J., Golovkin, I.E., Mancini, R.C., Welser, L.A., Bailey, J.E., Koch, J.A., Mehlhorn, T.A., Rochau, G.A., Wang, P. & Woodruff, P. (2005). Dopant radiative cooling

effects in indirect-drive Ar-doped capsule implosion experiments. *Phys. Rev. E* **72**, 066403.

Magelssen, G.R., Delamater, N.D., Lindman, E.L. & Hauer, A.A. (1998). Measurements of early time radiation asymmetry in vacuum and methane-filled Hohlraums with the reemission ball technique. *Phys. Rev. E* **57**, 4663.

Marinak, M.M., Kerbel, G.D., Gentile, N.A., Jones, O., Munro, D., Pollaine, S., Dittrich, T.R. & Haan, S.W. (2001). Three-dimensional HYDRA simulations of National Ignition Facility targets. *Phys. Plasmas* **8**, 2275–2280.

Meezan, N.B., Atherton, L.J., Callahan, D.A., Dewald, E.L., Dixit, S., Dzenitis, E.G., Edwards, M.J., Haynam, C.A., Hinkel, D.E., Jones, O.S., Landen, O., London, R.A., Michel, P.A., Moody, J.D., Milovich, J.L., Schneider, M.B., Thomas, C.A., Town, R.P.J., Warrick, A.L., Weber, S.V., Widmann, K., Glenzer, S.H., Suter, L.J., Macgowan, B.J., Kline, J.L., Kyrala, G.A. & Nikroo, A. (2010). National Ignition Campaign Hohlraum energetics. *Phys. Plasmas* **17**, 056304.

Merrill, F.E. (2015). Imaging with penetrating radiation for the study of small dynamic physical processes. *Laser Part. Beams* **33**, 425–431.

Murakami, M. (1992). Analysis of radiation symmetrization in hohlraum targets. *Nucl. Fusion* **32**, 1715–1724.

Murakami, M. & Meyer-Ter-Vehn, J. (1991). Radiation symmetrization in indirectly driven ICF targets. *Nucl. Fusion* **31**, 1333–1341.

Olson, R.E., Leeper, R.J., Nobile, A. & Oertel, J.A. (2003). Preheat effects on shock propagation in indirect-drive inertial confinement fusion ablator materials. *Phys. Rev. Lett.* **91**, 235002.

Ramirez, J., Ramis, R. & Meyer-Ter-Vehn, J. (1998). Integrated numerical simulation of indirect laser-driven implosion for ICF. *Laser Part. Beams* **16**, 91–99.

Ramis, R. (2013). Hydrodynamic analysis of laser-driven cylindrical implosions. *Phys. Plasmas* **20**, 082705.

Ramis, R., Meyer-Ter-Vehn, J. & Ramrez, J. (2009). MULTI2D-A computer code for two-dimensional radiation hydrodynamics. *Comput. Phys. Commun.* **180**, 977–994.

Ramis, R., Schmalz, R. & Meyer-Ter-Vehn, J. (1988). MULTI: A computer code for one-dimensional multigroup radiation hydrodynamics. *Comput. Phys. Commun.* **49**, 475–505.

Ramis, R., Temporal, M., Canaud, B. & Brandon, V. (2014). Three-dimensional symmetry analysis of a direct-drive irradiation scheme for the laser megajoule facility. *Phys. Plasmas* **21**, 082710.

Robey, H.F., Perry, T.S., Park, H.-S., Amendt, P., Sorce, C.M., Compton, S.M., Campbell, K.M. & Knauer, J.P. (2005). Experimental measurement of Au M-band flux in indirectly driven double-shell implosions. *Phys. Plasmas* **12**, 072701.

Schnittman, J.D. & Craxton, R.S. (1996). Indirect – drive radiation uniformity in tetrahedral hohlraums. *Phys. Plasmas* **3**, 3786–3797.

Simakov, A.N., Wilson, D.C., Yi, S.A., Kline, J.L., Clark, D.S., Milovich, J.L., Salmonson, J.D. & Batha, S.H. (2014). Optimized beryllium target design for indirectly driven inertial confinement fusion experiments on the National Ignition Facility. *Phys. Plasmas* **21**, 022701.

Varnum, W.S., Delamater, N.D., Evans, S.C., Gobby, P.L., Moore, J.E., Wallace, J.M., Watt, R.G., Colvin, J.D., Turner, R. & Glebov, V. (2000). Progress toward Ignition with Noncryogenic Double-Shell Capsules. *Phys. Rev. Lett.* **84**, 5153–5155.

https://doi.org/10.1017/S0263034617000258 Published online by Cambridge University Press